Statistical approach based on the Stoner-Wohlfarth model for the switching field in a misoriented magnet array

Donghyeon Lee,[1] Jungmin Park,[2,*] Donghyeon Han,[3] Suzuki Ippei,[4] Takahashi Yukiko,[4] Sujung Noh,[5] Jisung Lee,[5] JoonHyun Kwon,[5] Hansaem Lee,[5] and Sanghoon Kim[1,†]

[1] *Department of Physics, University of Ulsan, Ulsan 44610, Korea*
[2] *Department of Physics, KAIST, Daejeon 34141, Korea*
[3] *Materials Science and Engineering, KAIST, Daejeon 34141, Korea*
[4] *National Institute for Materials Science (NIMS), Tsukuba 305-0017, Japan*
[5] *Research & Development Division, Hyundai Motor Company, Hwaseong 18280, Korea*

(Received 27 September 2023; revised 18 December 2023; accepted 24 January 2024; published 13 February 2024)

The Stoner-Wohlfarth model (SW model) is used to explain the relationship between the external magnetic field and the magnetization reversal of a single magnetic domain. However, it is inappropriate for inhomogeneous magnetic films or bulk materials, such as granular and defective films, because the magnetization reversal of the films is affected by magnetic particles or grains, which could have a different anisotropy for uniaxial magnetic anisotropy (UMA) of the films. In this paper, we propose a model based on the SW model to understand the magnetization switching behavior of magnetic films with misoriented grains. Our model considers the distribution effect of different anisotropies originating from magnetic defects or domains against the UMA of a magnetic thin film, and a Gaussian function is employed for the probability distribution of tilted anisotropy. Finally, we experimentally demonstrate that our model describes the magnetic switching behavior of a granular magnetic film (FePt-C) with perpendicular magnetic anisotropy. This study provides an alternative analytical method for the magnetization reversal in magnetic devices.

DOI: 10.1103/PhysRevApplied.21.024027

I. INTRODUCTION

Over the last decade, the scaling down of ferromagnets has been an essential issue for high-density memory applications such as magnetoresistive random access memory (MRAM) and hard disk drives (HDD) [1–4]. By reducing the scale of a magnetic device with perpendicular magnetic anisotropy (PMA) up to tens of nanometers smaller than a single magnetic domain, the Stoner-Wohlfarth model (SW model) explains the switching behaviors of a device in a single domain state [5–7]. However, considering the wafer-scale fabrication for commercializing MRAMs, or the existence of nanometer-sized magnetic particles in the magnetic media of HDDs, the SW model cannot perfectly describe the total magnetization behaviors of billions of nanometer-sized ferromagnets for the following reasons [8–19]. In the cases of MRAM, magnetic properties inevitably degrade during device fabrication, such as etching damage at the edge of each device, resulting in different magnetic characteristics among magnetic tunnel junction (MTJ) devices on a 300-nm wafer. On the other hand, the magnetic media in HDDs consists of magnetic granular films such as FePt-SiO_2, FePt-C, and CoCrPt-SiO_2, in which the magnetic easy axes between particles are misoriented. The magnetic properties of granular films depend on grain size, grain interaction, and space between grains [20]. Therefore, the conventional SW model cannot provide representative information on nanosized pattern arrays or granular magnetic thin films. In addition to these systems, the magnetization behaviors of bulk hard magnets consisting of nanocomposites do not follow the SW model or the simple domain-wall propagation model [8,9] owing to the randomly oriented magnetic anisotropy of the composite in the magnets.

In this study, we develop a statistical model based on the SW model considering a situation in which the uniaxial magnetic anisotropy (UMA) direction of each particle in a system randomly deviates from the standard axis perpendicular to the plane. The statistical SW model reproduces the magnetization switching of a magnetic granular film, which has uncountable magnetic particles with a misorientation exhibiting strong PMA. The best fitting of the angle-dependent coercivity of the granular magnetic film (FePt-C) using the model quantitatively provided the degree of deviation of PMA. Our model can be practically

*jungmin0123@kaist.ac.kr
†sanghoon.kim@ulsan.ac.kr

utilized to analyze the magnetic properties of patterned or self-assembled magnetic arrays.

II. EXPERIMENTAL AND SIMULATION METHOD

A 4-nm-thick FePt-C nanogranular layer was epitaxially grown on a MgO (100) substrate by co-sputtering FePt and C targets. Pt (5 nm) was deposited as a capping layer. Here, the chemical composition of FePt was estimated to be approximately 50:50. A Hall bar geometry of the FePt-C thin film was defined by using photolithography and ion milling. The channel width and length of the device were 10 and 90 μm, respectively. Ru (100 nm) was employed as a contact pad for electrical measurement. All electrical measurements were performed in a cryogen-free measurement system (cryogenic LTD) with a source meter (Keithley 6221) and nanovoltmeter (Keithley 2182) at room temperature. An Al wire was used for electrical contact with the Ru pads of the device. A dc current of 1 mA was applied for electrical transport.

The micromagnetic simulation, MuMax3, was employed for comparison with our statistical model. In this simulation, the magnetic properties of FePt-C are referenced from Ref. [11]. The granular structure is developed by modified Voronoi tessellation with the perpendicular bisectors and asymmetric overlapping of the two layers as shown in Fig. 4(a). Here, unit cell and plane size are $1 \times 1 \times 1$ nm^3, and 200×200 nm^2, respectively. The thickness of the film is 4 nm. The average distance between grains (white shape) is 7 nm. We assume that magnetization saturation is 1.0×10^6 A/m, and the anisotropy constant is 5.0×10^6 J/m^3. Also, we consider the demagnetization effect in addition to a misorientation of the magnetic grains.

III. RESULTS AND DISCUSSION

A. Statistical model based on the SW model

The SW model considers two energies, the magnetic anisotropy and Zeeman energies in a single-domain ferromagnet. When an external magnetic field is applied, the total energy is given by [5,6],

$$E_{\text{tot}} = K_u \sin^2(\theta - \varphi) - \mu_0 M H_{\text{ex}} \cos\varphi, \tag{1}$$

where the K_u is the uniaxial anisotropy, M is the magnetization, and μ_0 is the vacuum permeability. The first and second terms indicate the contributions of the anisotropy energy and the Zeeman energy, respectively.

According to Eq. (1), the magnetization of a single domain rotates under an external magnetic field (H_{ex}) competing with K_u. The switching field (h_s) depends on the angle θ between the magnetic axis and H_{ex} as shown in Fig. 2(b). Then, the angle-dependent h_s for a single domain obtained from the minima of the Zeeman energy is given as [5]

$$h_s(\theta) = \frac{(1 - \tan^{2/3}\theta + \tan^{4/3}\theta)^{1/2}}{1 + \tan^{2/3}\theta}. \tag{2}$$

This is a solution from the conventional SW model to understand the magnetic switching behavior of a single domain.

Now, we consider a magnetic particle with another uniaxial anisotropy (K'_u), which is tilted from the K_u axis, as shown in Fig. 1. Although factors such as dipole-dipole interaction and domain wall can affect magnetization reversal by external magnetic field in the system with many magnetic domains or grains, we ignore these factors to focus on the statistic effect of tilted anisotropy of the grains. Then, a normalized magnetization vector with K'_u can be defined as follows:

$$n_x = \frac{\omega_x}{\sqrt{{\omega_x}^2 + {\omega_y}^2 + 1}}, n_y = \frac{\omega_y}{\sqrt{{\omega_x}^2 + {\omega_y}^2 + 1}}, n_z = \frac{1}{\sqrt{{\omega_x}^2 + {\omega_y}^2 + 1}}. \tag{3}$$

Here, ω is introduced to consider the tilted weight of K'_u. We set the z axis as the standard axis. Then, we can define the angle (δ) between K'_u and H_{ex} as in Eq. (4) because H_{ex} is applied in the x-z plane ($H_{\text{ex}} = (H\sin\theta, 0, H\cos\theta)$) as shown in Fig. 1(b).

$$H_{\text{ex}} \times \hat{n} = H\cos\delta = H\frac{\omega_x \times \sin\theta + \cos\theta}{\sqrt{{\omega_x}^2 + {\omega_y}^2 + 1}}. \tag{4}$$

The value of δ is determined by θ and $\omega_{x,y}$ as follows:

$$\cos\delta = \frac{\omega_x \times \sin\theta + \cos\theta}{\sqrt{{\omega_x}^2 + {\omega_y}^2 + 1}}. \tag{5}$$

If there is no difference between δ and θ, $\omega = 0$ because the directions of K_u and K'_u are the same as shown in Fig. 1(b). Therefore, h_s considered with the K'_u of the magnetic particles can be expressed as follows:

$$h_s(\delta(\theta, \omega_x, \omega_y)) = \frac{(1 - \tan^{2/3}(\delta(\theta,\ \omega_x,\ \omega_y)) + \tan^{4/3}(\delta(\theta,\ \omega_x,\ \omega_y)))^{1/2}}{1 + \tan^{2/3}(\delta(\theta,\ \omega_x,\ \omega_y))}. \tag{6}$$

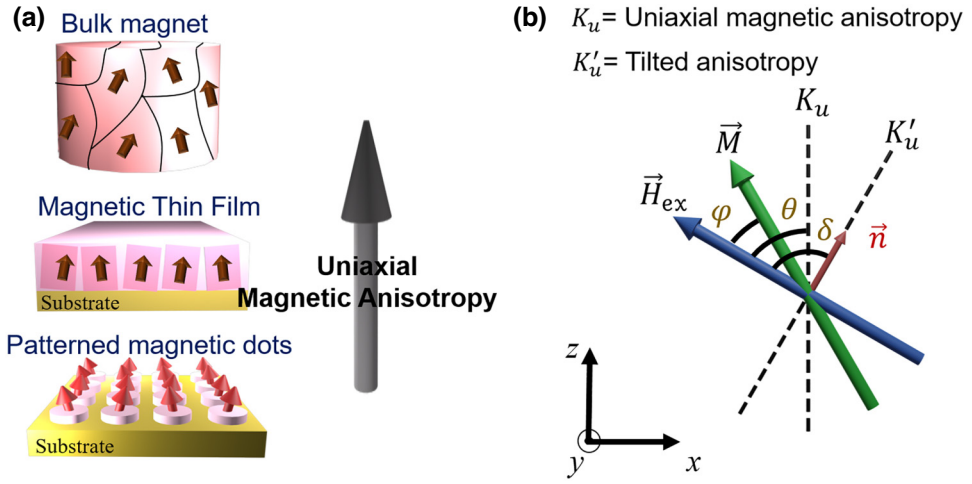

FIG. 1. Illustration of our model and the SW model. (a) In a magnetic device, magnetic grains can have different magnetic anisotropies. The red arrows indicate the anisotropy of a single domain. The black arrow indicates UMA. (b) Conceptualization of our model along with the SW model illustrating the magnetization of a single domain. φ indicates the angle of magnetization (M) indicating Zeeman energy. θ is the angle between the K_u of the UMA and $H_{\rm ex}$. δ is an angle related to the K_u' of magnetic particles against the UMA of the magnetic device.

Here, we set the values of ω_x and ω_y in the range of -5 to 5. In this range, the tilting angle $(\delta - \theta)$ of K_u' varies from -78.6° to 78.6° toward the x-y plane.

Figure 2 shows ω-dependent h_s determined using Eq. (6) in terms of θ when $-5 < \omega_{x,y} < +5$. To clarify our analytical calculation results, we first focus on h_s values as a function of ω_x and ω_y when $H_{\rm ex}$ is parallel to the normal direction to the x-y plane ($\theta = 0^\circ$). Here, δ is no longer a function of θ. Then, δ is only determined by $\omega_{x,y} = 0$ according to Eq. (5). The estimated h_s plot in

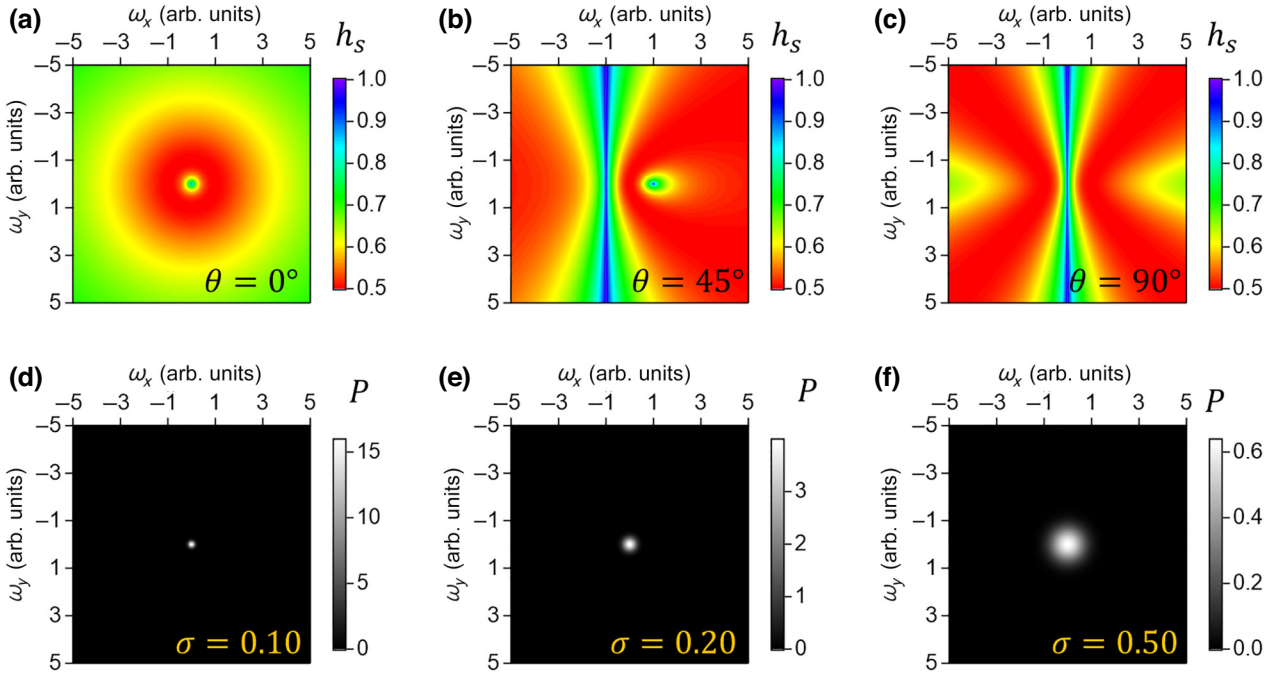

FIG. 2. Plot of ω-dependent h_s and P. h_s as a function of ω at $\theta = 0^\circ$ (a), 45° (b), and 90° (c) according to Eq. (7). The maximum value of h_s indicates the perpendicular between $H_{\rm ex}$ and the K_u' of magnetic particles. The Gaussian distribution as a function of t ω at $\sigma = 0.10$ (d), 0.20 (e), and 0.50 (f) from Eq. (7). The magnitudes of h_s and the probability distribution are expressed as a spectrum (the black color indicates the minimum values, and the white color indicates the maximum values).

Fig. 2(a) shows centrosymmetric behavior in terms of $\omega_{x,y}$. In the case of $\theta = 45^\circ$ in the x-z plane, the estimated h_s in terms of ω is noncentrosymmetric as shown in Fig. 2(b). When the K_u' axis is tilted by -45° from the z axis under $H_{\rm ex}$, $h_{\rm s}$ becomes maximum because K_u' is perpendicular to $H_{\rm ex}(\delta = 90^\circ)$. This behavior is natural according to the SW model. Therefore, the magnetization with $\omega_x = -1$ should have a maximum h_s independent of ω_y ($H_{\rm ex}$ is always orthogonal to the y axis) as shown in Fig. 2(b). If K_u' is parallel to $H_{\rm ex}$ indicating $\delta = 0$, the switching field can also have the maximum value. Hence, there is a peak when $\omega_x = 1$ and $\omega_y = 0$. Figure 2(c) shows the ω-dependent h_s values under $H_{\rm ex}$ with $\theta = 90^\circ$. This system also demonstrates the maximum value of h_s as the perpendicular ($\omega_x = 0$) and parallel ($\omega_x > 5, \omega_y = 0$) between $H_{\rm ex}$ and K_u', corresponding to the parabolic characteristic of h_s in the SW model well.

In the case of a system with several magnetic particles with various tilting angles ($\delta - \theta$) to the z axis, we introduce the probability distribution function in addition to the concept of ω. Here, we consider that the magnetic easy axis of each magnetic particle in the system has a random variable that depends on ω. Therefore, the Gaussian distribution, which is typically a continuous probability distribution function (P), was employed in our model as follows:

$$P(\omega_x, \omega_y) = \frac{1}{\sigma\sqrt{2\pi}} \exp\left(-\frac{1}{2}\left(\frac{\omega_x}{\sigma}\right)^2\right) \times \frac{1}{\sigma\sqrt{2\pi}} \exp\left(-\frac{1}{2}\left(\frac{\omega_y}{\sigma}\right)^2\right). \quad (7)$$

Here, σ is the standard deviation of P.

Figures 2(d)–2(f) indicate the ω-dependent $P(\omega_x, \omega_y)$ in terms of σ. Considering both P and ω, the expected value of h_s in the magnetic system for a large number of magnetic objects with various K_u' axes can be determined as

$$\langle h_s(\theta)\rangle = \sum_{\omega_x}\sum_{\omega_y} h_s(\delta(\theta, \omega_x, \omega_y))P(\omega_x, \omega_y). \quad (8)$$

To describe our model intuitively, the overlapping graph of h_s and P of magnetic particles is shown in Fig. 3(a) when θ is 45° and σ is 0.5 in Eq. (8). The dotted black circle indicates P with $\sigma = 0.5$ in Fig. 3(a). Then, the value of h_s in the magnetic system is expected to be within the probability distribution range because the ω of magnetic anisotropy, considering the range of standard deviation of the probability distribution, is directly related to the h_s of magnetic particles with different easy axis. In other words, the perspective of our model is how many particles, which have different h_s for each K_u', are distributed in the magnetic system.

Based on Eq. (8), the expected value of h_s as a function of θ with various values of σ is shown in Fig. 3(b). For the analytical calculation, the constraint range of ω is -5 to 5, which corresponds to $\delta \leq |81.95^\circ|$ at $\theta = 0^\circ$. In the case of the conventional SW model, the maximum value of h_s is obtained when $\theta = 0^\circ$ and 90°, and the minimum value is obtained when $\theta = 45^\circ$. On the other hand, the θ dependence of h_s weakens with increasing σ in our statistical SW model. As an increase in σ indicates that the range of the distribution of misoriented grains (the range of tilted weight) is widened, the expected value of h_s is less affected by θ. Therefore, h_s at $\theta = 45^\circ$ gradually increases with increasing σ as shown in Fig. 3(c). From Eq. (8), the θ for the minimum value of h_s is shifted from 45° to 20° with increasing σ as shown in Fig. 3(d).

B. Micromagnetic simulation

We also conduct the micromagnetic simulation to support our statistical SW model. Figure 4(a) shows the granular structure of a magnetic thin film with perpendicular magnetic anisotropy as mentioned in the experimental section. In addition to the concept of our statistical model, we incorporate the demagnetization effect of magnetic grains into the switching field. The θ dependence of the demagnetization field in each direction is shown in Fig. 4(b). Here, θ is defined as the angle between the magnetic axis and the external magnetic field in Fig. 1(b).

Figures 5(a)–5(e) indicate the magnetization as a function of the external magnetic field obtained from the micromagnetic simulation depending on σ and θ. Here, the magnetization is normalized with saturation magnetization. The key view in Figs. 5(a)–5(e) is that a perpendicular magnetic anisotropy becomes weaker as σ increases, meaning that each anisotropy of magnetic grains more tilts against uniaxial magnetic anisotropy of the magnetic granular films. From these results, we can obtain the h_s of the magnetic granular structure depending on various σ and θ. Figure 5(f) shows the angle dependence of h_s with our statistical SW model and the micromagnetic simulation. The squares indicate the results of the micromagnetic simulation, and the color dash lines show the statistical SW model. The micromagnetic simulations also show a tendency to increase the minimum h_s with increasing σ as in the statistical SW model [Fig. 3(b)].

C. Experimental results

To verify our analytical model, we applied it for the experimental observation of an FePt-C granular film [11], as shown in Figs. 6(a). FePt-C is a good template to evaluate our model because it contains large amounts of nanometer-sized magnetic particles with randomly distributed K_u' [21]. Figure 6(b) shows the normalized anomalous Hall effect (AHE) loops of the FePt-C granular film depending on the angle θ. The AHE loops exhibited a

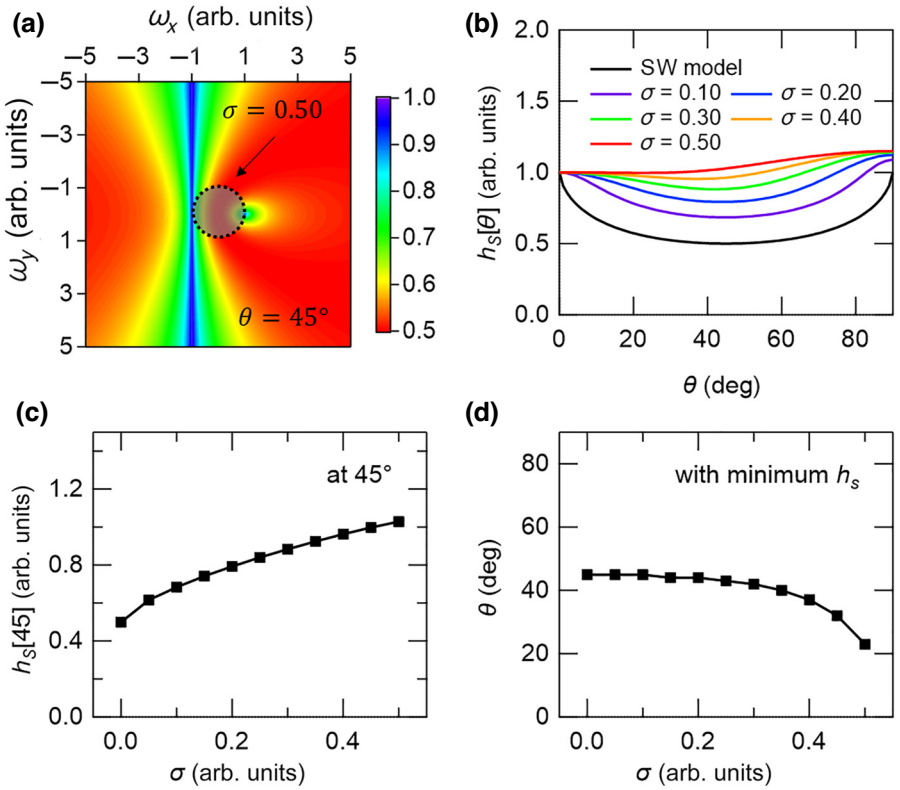

FIG. 3. Plot of expected values of h_s depending on σ. (a) Overlapping graph showing h_s and a Gaussian distribution with 95% uncertainty at $\theta = 45°$ and $\sigma = 0.5$ based on Eq. (8). The total value of h_s within the dotted black circle indicates the expected value of h_s under those conditions. (b) h_s as a function of θ with various values of σ. Increase in h_s with increasing standard deviation at $\theta = 45°$. (c) h_s at $\theta = 45°$ as a function of σ. Increase in the value of h_s with increasing σ. (d) Angle of minimum h_s versus the standard deviation. Decrease in θ with increasing σ.

typical PMA behavior. Figure 6(c) shows the normalized h_s of the granular film as a function of θ. Here, h_s was obtained from the coercive field of the AHE data. Unlike in the conventional SW model, the maximum value of h_s is observed at $\theta = 85°$, and the minimum value appears at $\theta = 30°$. The maximum and minimum h_s values are 1.2 and 0.8, respectively. That is, the h_s values of the FePt-C film do not exactly follow the SW model, as

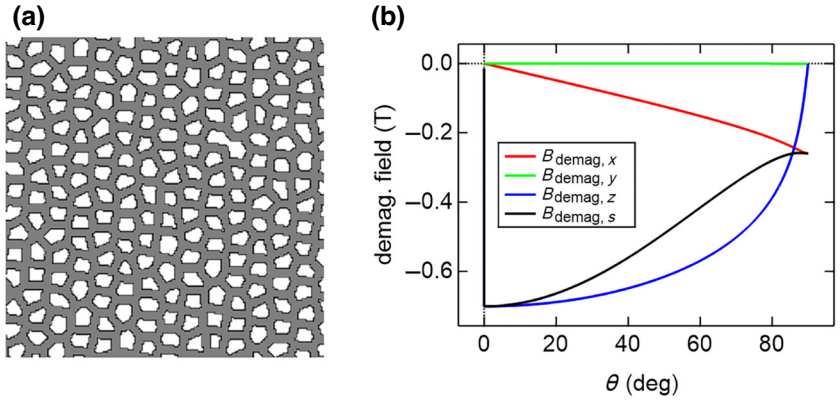

FIG. 4. Micromagnetic simulation for $h_s$of the granular magnetic film. (a) The image of a granular structure with perpendicular magnetic anisotropy. The white and gray colors in the structure indicate a magnetic material FePt and insulator C, respectively. This structure is created using modified Voronoi tessellation. (b) The angle dependence of the demagnetization field (B_{demag}) with each direction (x, y, z, s) in the granular structure. Here, s means the component parallel to saturation magnetization of the magnetic granular film ($B_{\text{demag},s} = B_{\text{demag},x}\sin(\theta) + B_{\text{demag},z}\cos(\theta)$) and the $B_{\text{demag},s}$ decrease as increasing with θ.

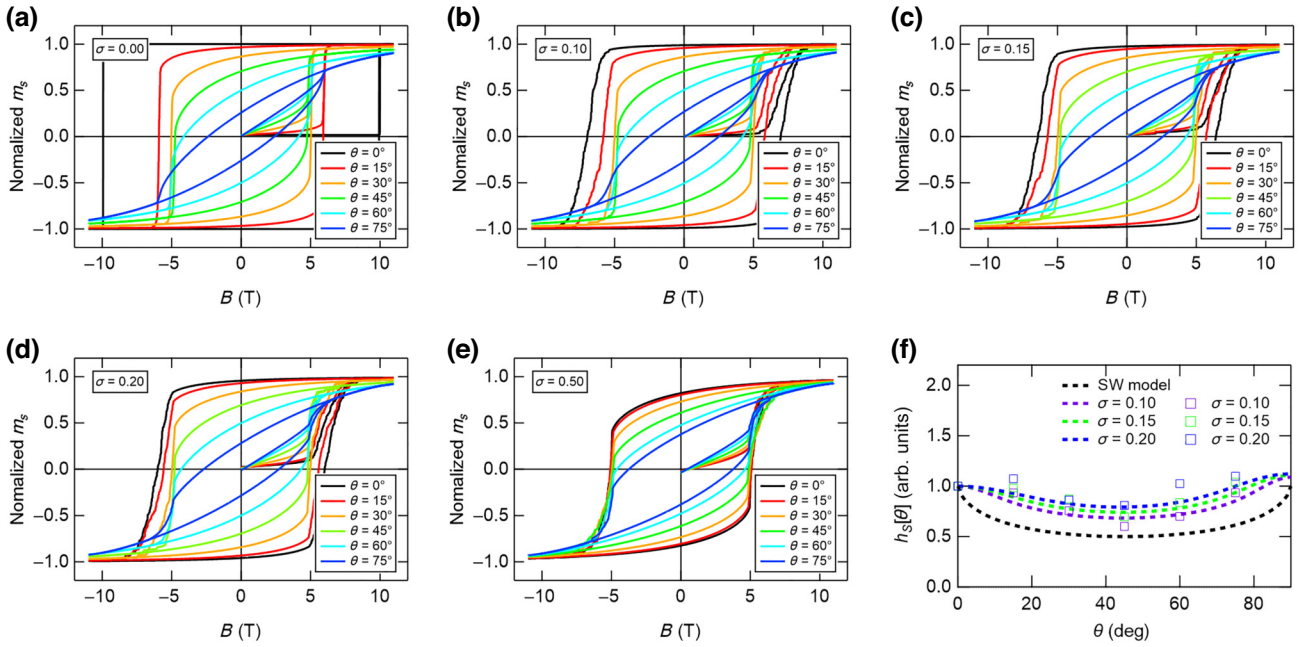

FIG. 5. The simulation results of the M-H curve with various angle θ. Magnetization as a function of a perpendicular magnetic field with $2K_U/M_S = 10$, where K_U is the anisotropy energy and M_S indicates the saturation magnetization, by (a) $\sigma = 0.00$ (meaning the SW model), (b) $\sigma = 0.10$, (c) $\sigma = 0.15$, (d) $\sigma = 0.20$, and (e) $\sigma = 0.50$. (f) The angle dependence of h_s obtained from our model and micromagnetic simulation. The dashed lines and squares indicate our statistical model and the micromagnetic simulation results, respectively. The black dashed line means the SW model. Simulation results of the granular structure are similar to our statistical model even though there is a demagnetization effect.

shown by the black dotted line in Fig. 6(c). This behavior has been reported for several magnetic granular systems [11–13]. Unlike the conventional SW model, our statistical SW model can fit the observed angle dependence of h_s when $\sigma = 0.15$ [see the blue dotted line in Fig. 6(c)]. The square indicates the data of the simulation in Fig. 6(c). The results of the simulation well describe our model and experiment although the demagnetization effect is included in the simulation condition. It means that the anisotropy of grains is dominant to the switching field in the magnetic granular film and our statistical SW model becomes particularly applicable when the magnetic anisotropy significantly surpasses the energy associated with interparticle interactions. Finally, we consider the dispersion weight of ω_x and the z axis to determine PMA properties to calculate a tilted angle $(\delta - \theta)$ of anisotropy of magnetic grains as shown in Fig. 6. Average tilted angle can be obtained from angle $\bar{\delta} = \sum_{\omega_x,\omega_y}^{\omega_x,\omega_y} \delta(\omega_x, \omega_y) \cdot P(\omega_x, \omega_y)$ and then, we can obtain the average value of the tilted angle depend on σ. In our statistical SW model, $\sigma = 0.15$ means

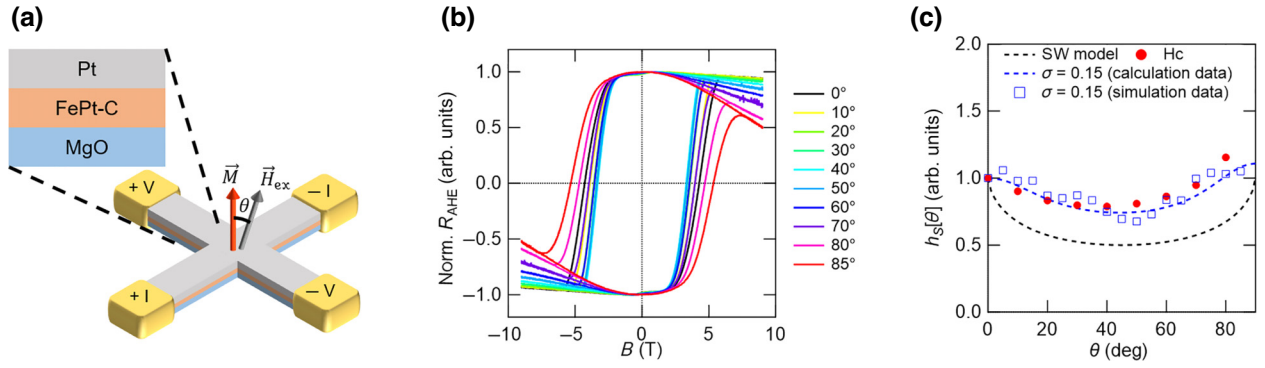

FIG. 6. Anomalous Hall effect of FePt-C granular film with PMA. (a) Illustration of the FePt-C Hall bar device. The AHE is measured at room temperature. (b) AHE as a function of the magnetic field B at various values of θ. The AHE loops are normalized. (c) The angle dependence of the coercive field of the FePt-C granular film. It is not fitted with the SW model (black dotted line).

$\omega\left(\left|\sqrt{\omega_x^2+\omega_y^2}\right|\right) = 0.187966$. This value indicates that the magnetic anisotropy in this FePt-C granular film is tilted by 10.8358° (on average) from the z axis.

D. Discussion

The conventional SW model explains the magnetization behavior of a particle with a single-domain state under H_{ex}. Here, we added two factors to apply the SW model to real situations as follows. First, we consider a system with multiple particles. Second, we add an additional frame K_u' to the frame of the conventional SW model, as shown in Fig. 1(b). Tilted magnetic anisotropy against UMA has been an issue because it is related to the magnetic characteristics in various magnetic systems. Fischbacher *et al.* [22] theoretically showed that the misorientation of the anisotropy axis, which is caused by the demagnetizing field at the grain boundary, affects the reduction in the coercive field by nucleation in permanent magnets. This misorientation effect is more dominant than the thermal fluctuation. In addition, the misoriented grains in a hard magnet influence local magnetization switching [23,24]. In the case of magnetic thin films, misoriented grains are formed primarily at the interface between the magnetic thin film and the substrate [21,25,26], and at grain boundaries [27]. For example, strain relaxation occurs in an FePt film deposited on a TiN substrate, leading to the formation of misoriented FePt grains [28]. This induces a change in the coercive field of the FePt film. As mentioned in the Introduction section, the tilted anisotropy of the magnetic grains decreases the thermal stability of an MTJ, which is a unit device in MRAM. This is because tilted magnetic grains weaken the UMA of magnetic thin films [29,30]. As this thermal stability is related to the write and read error rate, our statistical SW model can be used to evaluate the magnetic properties of magnetic pattern arrays and those of magnetic granular films for ultra-high-density magnetic recording media toward achieving tens of terabits per square inch [31–34].

Meanwhile, previous results based on the SW model cannot explain the angle dependence of the switching field around 90° [35,36]. To overcome these limitations, the distribution of magnetization was considered on saturation magnetization and hysteresis loop [37,38]. However, the aforementioned problem with high angle has not been fully solved yet because a polar angle is solely considered. However, we statistically deal with Gaussian-type distribution in the magnetic easy axis considering an azimuthal angle as well as the polar angle as shown in Figs. 2 and 3. Our model and micromagnetic simulation reproduce the switching field within a full range of the external field angle in Fig. 6(c). Therefore, we attribute our results of switching field around 90° to the Gaussian-type distribution with an azimuthal and polar angle.

IV. SUMMARY

In this study, we introduce a statistical method for different anisotropy effects to analyze the magnetization reversal of magnetically inhomogeneous arrays extending the SW model. The expected value of h_s calculated by our model well reproduces the experimentally observed angle dependence of the coercivity of the granular film. The statistical SW model can be widely applied for the quantitative analyses of the magnetic characteristics of various magnetic array systems or bulk-hard magnets.

ACKNOWLEDGMENTS

We acknowledge Grant No. NRF-2019R1C1C1010345 from the Samsung Research Funding Center of Samsung Electronics under Project No. SRFC-IT1901-11. J. Park acknowledges the support of the National Research Foundation of Korea grant funded by the Korea government (MSIT) (Grant No. NRF-2022R1C1C2010737). This work was supported by the Hyundai Motor Company.

[1] Q. Cao, W. Lü, X. R. Wang, X. Guan, L. Wang, S. Yan, T. Wu, and X. Wang, Nonvolatile multistates memories for high-density data storage, ACS Appl. Mater. Interfaces **12**, 42449 (2020).

[2] A. Hirohata, K. Yamada, Y. Nakatani, I.-L. Prejbeanu, B. Diény, P. Pirro, and B. Hillebrands, Review on spintronics: Principles and device applications, J. Magn. Magn. Mater. **509**, 166711 (2020).

[3] M. A. Khan, J. Sun, B. Li, A. Przybysz, and J. Kosel, Magnetic sensors - a review and recent technologies, Eng. Res. Express **3**, 022005 (2021).

[4] O. Gutfleisch, M. A. Willard, E. Brück, C. H. Chen, S. G. Sankar, and J. P. Liu, Magnetic materials and devices for the 21st century: Stronger, lighter, and more energy efficient, Adv. Mater. **23**, 821 (2011).

[5] E. C. Stoner and E. P. Wohlfarth, A mechanism of magnetic hysteresis in heterogeneous alloys, Philos. Trans. R. Soc. London A **240**, 599 (1948).

[6] C. Tannous and J. Gieraltowski, The Stoner–Wohlfarth model of ferromagnetism, Eur. J. Phys. **29**, 475 (2008).

[7] A. Stancu and C. Papusoi, Hysteresis modeling of recording media with as interacting Stoner-Wohlfarth particles system, IEEE Trans. Magn. **30**, 4308 (1994).

[8] M. F. de Campos, S. A. Romero, F. J. G. Landgraf, and F. P. Missell, Estimate of the anisotropy field in isotropic $SmCo_2$: 17 magnets with the Stoner-Wohlfarth CLC model, J. Phys.: Conf. Ser. **303**, 012049 (2011).

[9] E. Girt, K. M. Krishnan, G. Thomas, E. Girt, and Z. Altounian, Coercivity limits and mechanism in nanocomposite Nd–Fe–B alloys, J. Magn. Magn. Mater. **231**, 219 (2001).

[10] T. Schrefl, H. F. Schmidts, J. Fidler, and H. Kronmüller, The role of exchange and dipolar coupling at grain boundaries in hard magnetic materials, J. Magn. Magn. Mater. **124**, 251 (1993).

[11] H. Pandey, J. Wang, T. Shiroyama, B. S. D. Ch, S. Varaprasad, H. Sepehri-Amin, Y. K. Takahashi, A. Perumal, and K. Hono, Structure optimization of FePt–C nanogranular films for heat-assisted magnetic recording media, IEEE Trans. Magn. **52**, 1 (2016).

[12] S. Wicht, V. Neu, L. Schultz, D. Weller, O. Mosendz, G. Parker, S. Pisana, and B. Rellinghaus, Atomic resolution structure–property relation in highly anisotropic granular FePt-C films with near-Stoner-Wohlfarth behaviour, J. Appl. Phys. **114**, 063906 (2013).

[13] M. C. dos Santos, J. Geshev, J. E. Schmidt, S. R. Teixeira, and L. G. Pereira, Origin of the magnetization reversal of an Fe thin film on Si(111), Phys. Rev. B **61**, 1311 (2000).

[14] S. Tibus, T. Strache, F. Springer, D. Makarov, H. Rohrmann, T. Schrefl, J. Fassbender, and M. Albrecht, Magnetic properties of granular CoCrPt : SiO_2 films as tailored by Co^+ irradiation, J. Appl. Phys. **107**, 093915 (2010).

[15] S. K. Srivastava, R. Hussain, T. Hauet, and L. Piraux, Magnetization reversal and switching field distribution in Co-Tb based bit patterned media, AIP Conf. Proc. **2115**, 030482 (2019).

[16] F. Nguyen-Van-Dau, M. Sussiau, A. Schuhl, and P. Galtier, Magnetic thin films having a lateral nanostructural periodicity, J. Appl. Phys. **81**, 4482 (1997).

[17] J. Lee, C. Brombacher, J. Fidler, B. Dymerska, D. Suess, and M. Albrecht, Contribution of the easy axis orientation, anisotropy distribution and dot size on the switching field distribution of bit patterned media, Appl. Phys. Lett. **99**, 062505 (2011).

[18] J. W. Lau, X. Liu, R. C. Boling, and J. M. Shaw, Decoupling nucleation and domain-wall propagation regimes in $(Co/Pd)_n$ multilayer nanostructures, Phys. Rev. B **84**, 214427 (2011).

[19] Bernard Dieny, Mair Chshiev, Brian Charles, Nikita Strelkov, Alain Truong, Olivier Fruchart, Ali Hallal, Jian Wang, Yukiko K. Takahashi, Tomohito Mizuno, and Kazuhiro Hono, Impact of intergrain spin-transfer torques due to huge thermal gradients in heat-assisted magnetic recording, IEEE Trans. Magn. **54**, 1 (2018).

[20] S. Ohnuma, H. Fujimori, S. Mitani, and T. Masumoto, High-frequency magnetic properties in metal–nonmetal granular films (invited), J. Appl. Phys. **79**, 5130 (1996).

[21] J. Wang, S. Hata, Y. K. Takahashi, H. Sepehri-Amin, B. S. D. Ch, S. Varaprasad, T. Shiroyama, T. Schrefl, and K. Hono, Effect of MgO underlayer misorientation on the texture and magnetic property of FePt–C granular film, Acta Mater. **91**, 41 (2015).

[22] J. Fischbacher, A. Kovacs, L. Exl, J. Kühnel, E. Mehofer, H. Sepehri-Amin, T. Ohkubo, K. Hono, and T. Schrefl, Searching the weakest link: Demagnetizing fields and magnetization reversal in permanent magnets, Scr. Mater. **154**, 253 (2018).

[23] M. Gusenbauer, H. Oezelt, J. Fischbacher, A. Kovacs, P. Zhao, T. G. Woodcock, and T. Schrefl, Extracting local nucleation fields in permanent magnets using machine learning, npj Comput. Mater. **6**, 89 (2020).

[24] L. Exl, J. Fischbacher, A. Kovacs, H. Özelt, M. Gusenbauer, K. Yokota, T. Shoji, G. Hrkac, and T. Schrefl, Magnetic microstructure machine learning analysis, J. Phys. Mater. **2**, 014001 (2018).

[25] J. Wang, H. Sepehri-Amin, Y. K. Takahashi, T. Ohkubo, and K. Hono, Magnetic in-plane components of FePt nanogranular film on polycrystalline MgO underlayer for heat-assisted magnetic recording media, Acta Mater. **177**, 1 (2019).

[26] A. Berger, Magnetization reversal in granular thin films, Phys. B **407**, 1322 (2012).

[27] J. Ye, W. He, Q. Wu, H.-L. Liu, X.-Q. Zhang, Z.-Y. Chen, and Z.-H. Cheng, Determination of magnetic anisotropy constants in Fe ultrathin film on vicinal Si(111) by anisotropic magnetoresistance, Sci. Rep. **3**, 1 (2013).

[28] H. H. Li, K. F. Dong, J. F. Hu, T. J. Zhou, G. M. Chow, and J. S. Chen, Lattice relaxation and its impact on magnetic properties of FePt thin film, J. Phys. D: Appl. Phys. **46**, 015002 (2012).

[29] S.-W. Chung, *et al.*, in *2016 IEEE International Electron Devices Meeting (IEDM)* (IEEE, 2016), pp. 27.1.1–27.1.4.

[30] Sadahiko Miura, Koichi Nishioka, Hiroshi Naganuma, T. V.A. Nguyen, Hiroaki Honjo, Shoji Ikeda, Toshinari Watanabe, Hirofumi Inoue, Masaaki Niwa, Takaho Tanigawa, Yasuo Noguchi, Toru Yoshizuka, Mitsuo Yasuhira, and Tetsuo Endoh, Scalability of quad interface P-MTJ for 1X Nm STT-MRAM with 10-Ns low power write operation, 10 years retention and endurance $>10^{11}$, IEEE Trans. Electron Devices **67**, 5368 (2020).

[31] B. S. D. Ch. S. Varaprasad, J. Wang, T. Shiroyama, Y. K. Takahashi, and K. Hono, Columnar structure in FePt–C granular media for heat-assisted magnetic recording, IEEE Trans. Magn. **51**, 1 (2015).

[32] H. Pandey, A. Perumal, J. Wang, Y. K. Takahashi, and K. Hono, Growth mechanism of columnar grains in FePt–C granular films for HAMR media processed by compositionally graded sputtering, IEEE Trans. Magn. **52**, 1 (2016).

[33] A. Perumal, Y. K. Takahashi, and K. Hono, FePt–C nanogranular films for perpendicular magnetic recording, J. Appl. Phys. **105**, 07B732 (2009).

[34] S. Chen, X. Shu, Q. Xie, C. Zhou, J. Zhou, J. Deng, R. Guo, Y. G. Peng, G. Ju, and J. Chen, Structure, magnetic and thermal properties of FePt–C–BN granular films for heat assisted magnetic recording, J. Phys. D: Appl. Phys. **53**, 135002 (2020).

[35] T. Thomson, K. R. Coffey, and J.-U. Thiele, Angle-dependent switching of granular and multilayer perpendicular media, IEEE Trans. Magn. **39**, 5 (2003).

[36] J.-L. Tsai, J.-Y. Chen, C. Dai, T.-W. Hsu, and S.-M. Weng, Surface and microstructure analysis of CoCrPt film on RuCoCrX (X = Ti, Re) intermediate layers, Crystals **10**, 263 (2020).

[37] A. Kuncser and V. Kuncser, Magnetization reversal via a Stoner–Wohlfarth model with bi-dimensional angular distribution of easy axis, J. Magn. Magn. Mater. **395**, 34 (2015).

[38] M. F. de Campos, F. A. S. da Silva, E. A. Perigo, and J. A. de Castro, Stoner–Wohlfarth model for the anisotropic case, J. Magn. Magn. Mater. **345**, 147 (2013).